EasyChair Preprint

№ 13974

Analysis of the Storage and Release of Thermal Solar Energy for the Production of Domestic Hot Water Using Encapsulated PCM

Cristina Bianqui, Antonio Viedma, Alberto Egea and Alberto García

July 15, 2024

ANALYSIS OF THE STORAGE AND RELEASE OF THERMAL SOLAR ENERGY FOR THE PRODUCTION OF DOMESTIC HOT WATER USING ENCAPSULATED PCM

C Bianqui,[a,*], A Viedma [a], A Egea [a] and A García [a]
[a] Universidad Politécnica de Cartagena, Departamento de Ingeniería Térmica y de Fluidos, Escuela Técnica Superior de Ingeniería Industrial. Campus Muralla del Mar, Calle Doctor Fleming, s/n, 30202 Cartagena, España.
*cristina.bianqui@edu.upct.es

Abstract: In recent years, the need for energy storage has become more noteworthy, leading to the development of thermal energy storage (TES) systems. In this study, the phase change processes of encapsulated PCM used in hybrid accumulators in domestic hot water systems are analyzed. The PCM used is RT35HC paraffin from the manufacturer Rubitherm, and a study of its properties is conducted. The encapsulation is cylindrical and made of stainless steel, with either a temperature probe inserted into the encapsulation to measure the temperature field, a transparent cover to visualize the interior, or both. This allows for an assessment of the measurement methods used and a preliminary understanding of the behavior of the encapsulated PCM. Subsequently, melting and solidification tests are conducted, simulating the charging and discharging processes of the accumulator, respectively. The encapsulation is placed in both vertical and horizontal positions. Based on these tests, the heat flux exchanged and the energy accumulated in the stainless-steel encapsulation are obtained.

Keywords: encapsulated PCM, thermal energy storage, solar systems efficiency, solar energy, domestic hot water

1. INTRODUCTION

Over the past two decades, global energy consumption and CO_2 emissions have significantly risen, as reported in the Renewables 2022 Global Status Report. Furthermore, the residential sector accounts for roughly one-third of total energy consumption, of which around 70% is used for water and building heating. These applications are suitable for renewable energy sources, particularly solar energy.

The expansion of solar domestic hot water (DHW) systems is notable due to their cost-effectiveness and sustainability for residential energy needs. These systems utilize solar thermal collectors to absorb sunlight and heat water for DHW production and space heating, significantly reducing energy costs and greenhouse gas emissions. However, their effectiveness is challenged by solar energy intermittency, making energy storage crucial.

Thermal energy storage (TES) systems, particularly those using phase change materials (PCM), have been developed to enhance DHW system efficiency. Hybrid accumulators, which combine water and encapsulated PCM, have been designed and manufactured. These systems are known for their easy manufacturing, suitability for domestic use and cost-effectiveness. Hybrid accumulators commonly incorporate macroencapsulated PCM in a packed-bed configuration.

In recent literature, both numerical and experimental studies on hybrid packed-bed accumulators have been explored, with numerical studies being more prevalent due to their flexibility in modifying system conditions and encapsulation geometries. For instance, Veerappan et al. (2009) examined the phase change processes of various PCMs in spherical encapsulations, analyzing the impact of encapsulation size and the initial temperatures of the PCM and heat-transfer fluid, remarking the importance of this kind of analysis when choosing the optimal encapsulation for a TES system. A notable configuration is the cascade hybrid accumulator, which incorporates encapsulations of different phase change materials, such as in the studies done by Yang et al. (2014) and Majumdar and Saha (2020). Both studies found that this configuration enhances energy performance compared to single PCM systems and improves the efficiency of the solar collectors of the system. In our research group, the design and manufacturing of a hybrid accumulator with cylindrical stainless-steel encapsulations have previously been done (Hernández Ballester, 2023).

Spherical encapsulations are the most common in hybrid accumulators, but other geometries have been studied. Kumar and Saha (2022) developed a mathematical model for a packed-bed system with cylindrical micro-encapsulations since cylinders can optimize the phase change processes due to their higher area-to-volume ratio. Xu et al. (2022) studied ellipsoidal polypropylene encapsulations experimentally and numerically, concluding that they are more suitable for applications requiring rapid charge and discharge processes.

Nevertheless, understanding the behavior of a single encapsulation is essential for maximizing system efficiency. Archibold et al. (2014) conducted numerical studies on temperature fields and liquid PCM currents in a nickel spherical encapsulation using NaNO3 as PCM. Li et al. (2015) used thermocouples to study the temperature field inside a paraffin-filled sphere during charge and discharge tests. Issa and Thirunavukkarasu (2024) found copper cylinders had the shortest discharge time and highest efficiency in a parabolic solar collector setup, comparing with other geometries and materials. Cheng and Zhai (2017) studied the behavior of PCM inside red blood cell-shaped nylon encapsulations, resulting them to outperform other geometries.

The technique of inserting thermocouples can be invasive, as explained by Tan in 2008, who compared the constrained and unconstrained melting process. Consequently, other techniques have been developed. Assis et al. (2007) used a spherical glass encapsulation with paraffin to compare numerical and experimental results of the PCM melting pattern without being altered. Boroojerdian et al. (2023) used a visualization method to study the PCM behavior in a copper cylinder, capturing images over time through a glass cover. Teather and Siddiqui (2023) measured the encapsulated PCM temperature using an infrared camera in a methacrylate encapsulation.

Given the scarcity of experimental studies of encapsulated PCM and the limited information currently available in the literature, in the present study an analysis of the phase change processes of encapsulated PCM is done. A stainless-steel cylinder is chosen for the encapsulation. The PCM used in this study is RT35HC paraffin from the manufacturer Rubitherm, and its properties are studied in this research. Regarding the tests, firstly an initial assessment of the measurement methods used in this study is performed. Subsequently, the temperature data are analyzed by calculating the heat flux exchanged and the energy accumulated and released during the PCM melting and solidification processes.

2. MATERIALS AND METHODS

2.1. Experimental setup

A scheme of the experimental setup for conducting the melting and solidification tests is presented in Fig. 1. The setup includes two thermal baths. The first one (1) is a thermal bath from the manufacturer JP SELECTA S.A (VB-1423 model). It is a cylindrical glass vessel (outer diameter of 300 mm and height of 320 mm). The second bath (2) is a thermostatic bath from the manufacturer SHOTT IBERICA (model CT-52). It is a rectangular methacrylate bath (375 x 215 x 325 mm) which is equipped with a thermostat to control the water temperature. The encapsulation containing the PCM (3) is placed in this bath.

A multipoint probe (4) with 6 type-T thermocouples is inserted into the encapsulation to measure the PCM temperature values. These thermocouples have been previously calibrated, to improve its accuracy from 1 to 0.1 ºC. A PT100 class B 1/10 DIN sensor (5) is placed in the thermal bath to measure the water temperature. It has an accuracy of 0.03 ºC. Both the multipoint probe and the PT100 sensor are connected to the data acquisition system 34980A model from Agilent Technologies (6) so as to obtain all the data. The computer (7) is used for data post-process.

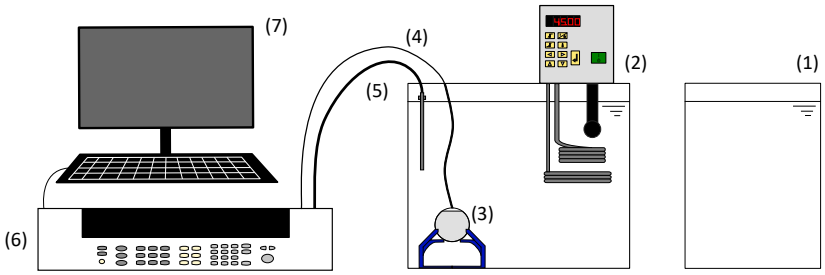

Figure 1. Experimental setup for melting and solidification tests

2.2. Geometry of the encapsulations

In this research, the aim is to study and understand more deeply the behavior of the PCM inside the encapsulation and to determine the effects of different measurement methods on the PCM. For these reasons, three encapsulations have been manufactured. All of them have a cylindrical shape. The first encapsulation is made entirely of stainless steel. Its geometry is shown in Fig. 2a. The encapsulation is manufactured from a tube with a width of 20 mm, an outer diameter of 60.3 mm, and a thickness of 1.5 mm. It is sealed with two plates of the same thickness and diameter as the tube, serving as covers on both ends of the tube. In one of the plates, three holes are made. These are indicated in Fig. 2a with thinner lines. The medium-sized hole is used to fill the capsule with liquid PCM using a syringe up to its maximum volume, which is 40 ml. The smallest hole allows air to escape during the filling process, as it is impossible to completely fill the encapsulation with PCM, so an air gap remains. The largest hole is used to insert a multipoint probe into the encapsulation so the PCM temperature can be measured.

The positions of the 6 type-T thermocouples of the probe are shown in Fig. 2a as well. It is observed that the thermocouples are arranged in a semicircumference with a radius of 15 mm, with one of them positioned at the centre. This arrangement is based on the assumption that the temperature field is symmetric throughout the encapsulation. The thermocouples are located in the middle plane of the encapsulation, at 10 mm from the plates. This is considered to be the most representative region to measure the PCM temperature. A three-dimensional scheme of the location of the sensors inside the encapsulation is observed in Fig. 2b. In Fig. 3a, a photography of the stainless-steel encapsulation is included.

The second encapsulation, shown in Fig. 3b, is a copy of the previous one, except that one of the plates has been replaced by a transparent methacrylate cover. This modification allows the observation of the PCM behavior during the tests. The last encapsulation, shown in Fig. 3c, also has a transparent cover, but the multipoint probe and the largest hole have been removed. The objective of this design is to compare the PCM melting pattern that is seen through the transparent cover in both encapsulations, with and without probe.

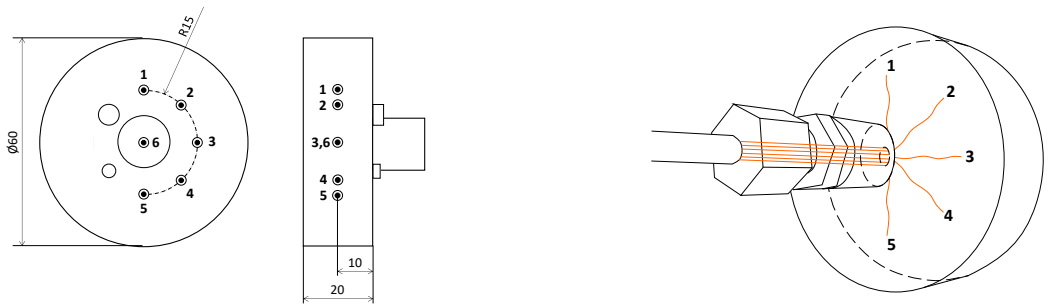

a) b)

Figure 2. Scheme of the encapsulation and the position of the thermocouples (dimensions in mm): a) 2D b) 3D

a) b) c)

Figure 3. Photographs of the three encapsulations: a) Stainless-steel encapsulation with probe b) Transparent encapsulation with probe c) Transparent encapsulation without probe

2.3. PCM properties

Paraffin RT35HC from the manufacturer Rubitherm is used as PCM in this study. To obtain more accurate values than those provided by the manufacturer, its thermal properties have been measured experimentally. Both the manufacturer and experimental values are detailed in Table 1.

The melting and solidification temperature ranges and heat storage capacity are determined using Differential Scanning Calorimetry (DSC) with the Mettler Toledo DSC822e equipment with a 6.65 mg sample. Figure 4 presents the energy released during solidification (black line) and the energy stored during melting (red line) over temperature.

During both melting and solidification, the presence of two peaks is noticed in the curves. The lower peak corresponds to a solid-solid transformation of the paraffin, involving crystal rearrangement, whereas the higher value peak represents the phase change, as explained by Kahwaji et al. (2018). Both peaks are considered when calculating the heat storage capacity. This calculation consists of integrating the area under each curve. These values differ slightly due to phase change hysteresis according to Liu et al. (2022).

Temperature ranges are obtained by drawing tangent lines at the point of maximum slope (blue lines). It is observed that both ranges differ from the manufacturer values and the solidification range is lower than the melting range which is a typical behavior of paraffins as described by Mekaddem et al. (2024).

The specific heat capacity is also obtained with DSC analysis. The test is conducted based on the enthalpy graphs, according to the temperature ranges where melting and solidification occur. Thus, the specific heat capacity is measured for temperature values between 15 and 50 ºC and it is calculated as the average of the values outside the phase change range.

The solid density was measured with a helium stereopycnometer with the SPY-D160-E equipment from Quantachrome Instruments, while liquid density was obtained by measuring mass and volume values with a syringe. In Table 1 it is seen that density in both phases are practically the same as the manufacturer values.

Table 1. Thermal properties of the paraffin RT35.

Thermal characteristics [units]	Manufacturer values	Experimental values
Melting temperature [ºC]	34-36	32-38
Solidification temperature [ºC]	36-34	35-27
Melting heat storage capacity [J/ kg]	240000	233700
Solidification heat storage capacity [J/ kg]	240000	237500
Specific heat capacity [J/ (kg·ºC)]	2000	1900
Solid density at 25ºC [kg/ m^3]	880	880
Liquid density at 45 ºC [kg/ m^3]	770	790

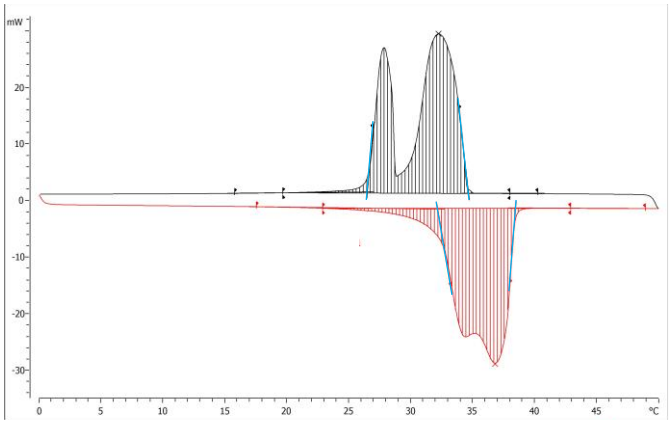

Figure 4. DSC analysis results

2.4. Equations

The following equations are analogous for both phase change (*pc* for the subscript) processes, melting and solidification. With the temperature data, the liquid fraction of PCM in the encapsulation at a given time instant *i* for each sensor *j*, $LF_{i,j}$, can be calculated using Eq. (1), where $T_{i,j}$ is the temperature in a time instant *i* for the sensor *j* and $T_{pc,lower}$ and $T_{pc,upper}$ are the lower and upper phase change temperature, respectively. It has been assumed that the liquid fraction is linear with the temperature during the phase change. Then, the liquid fraction in every time instant, LF_i, is calculated with Eq. (2).

$$\begin{aligned} LF_{i,j} &= 0 && \text{if} \quad T_{i,j} < T_{pc,lower} \\ LF_{i,j} &= \frac{T_{i,j} - T_{pc,lower}}{T_{pc,upper} - T_{pc,lower}} && \text{if} \quad T_{pc,lower} < T_{i,j} < T_{pc,upper} \\ LF_{i,j} &= 1 && \text{if} \quad T_{i,j} > T_{pc,upper} \end{aligned} \tag{1}$$

$$LF_i = \sum_{j=1}^{n} LF_{i,j}\ A_{f,j} \tag{2}$$

Where *n* is the total number of sensors in the encapsulation and $A_{f,j}$ represents the area fraction assigned to each sensor, as it has been assumed that the temperature of each sensor represents a sector of the encapsulation due to the limited number of sensors. There are 9 sensors in total, as symmetry is imposed on sensors 2, 3 and 4.

Thereafter, the stored and released energy is calculated. Equation (3) presents a method for calculating the global energy, E_{global}, during phase change processes, where sensible and latent energy of the PCM and the energy of the steel are considered.

$$E_{global} = m_{PCM}\left(c_{PCM}\left(T_{final} - T_{initial}\right) + L_{pc}\right) + m_{steel}\ c_{steel}\left(T_{final} - T_{initial}\right) \tag{3}$$

Where the index *PCM* refers to the properties of the PCM and *steel* to the properties of the stainless-steel. The index *m* refers to the melting process and the index *s* refers to the solidification process. *m* is the mass, *c* is the specific heat capacity, L_{pc} is the heat storage capacity and $T_{initial}$ and T_{final} are the temperatures at the initial and final instant of each test, respectively. This way, an order of magnitude for the expected value of energy is determined.

An alternative method to calculate the energy during the tests is computed based on the temperature of each sensor. This consists of calculating first the heat flux of the PCM, $\dot{Q}_{i,j}$, and then its energy by integrating. After that, the energy stored or released of the steel is added.

Hence, in Eq. (4) the first row represents the calculation of the latent heat flux, in which the variation of the PCM mass during the phase change with respect to temperature, $\frac{dm_{PCM,pc}}{dT}$, is considered. This is calculated based on the liquid fraction, resulting in a constant value due to the assumption of the linearity of the liquid fraction with temperature. The second row of Eq. (4) shows the sensible heat flux. The variation of the temperature with respect to time, $\frac{dT}{dt}_{i,j}$, is considered in both equations.

$$\begin{aligned} \dot{Q}_{i,j} &= \frac{dm_{PCM,pc}}{dT} A_{f,j} L_{pc} \frac{dT}{dt}_{i,j} + m_{PCM} A_{f,j} c_{PCM} \frac{dT}{dt}_{i,j} && \text{if} \quad T_{pc,lower} < T_{i,j} < T_{pc,upper} \\ \dot{Q}_{i,j} &= m_{PCM} A_{f,j} c_{PCM} \frac{dT}{dt}_{i,j} && \text{if} \quad T_{i,j} < T_{pc,lower} \text{ or } T_{i,j} > T_{pc,upper} \end{aligned} \tag{4}$$

The heat flux exchanged in every time instant, $\dot{Q}_i$, is the sum of the heat flux of each sensor in that specific time instant (Equation (5)). Subsequently, the total stored or released energy during the melting or solidification process, $E_{PCM,integrated}$, respectively, is calculated with Eq. (6).

$$\dot{Q}_i = \sum_{j=1}^{n} \dot{Q}_{i,j} \tag{5}$$

$$E_{PCM,integrated} = \int_{t_{process}} \dot{Q}_i \, dt \tag{6}$$

2.5. Experimental procedure

In this study, both melting and solidification tests have been conducted. The melting tests simulate the charging processes of the accumulator, when energy is stored. To have a first assessment of the experimental procedure used in the tests, an initial series of tests is conducted, in which the temperature rises to a certain value. The procedure involves placing the encapsulation in the rectangular bath filled with water at ambient temperature (approximately 25 ºC) and then heating the water to 45 ºC. All three encapsulations are used in these tests.

Afterwards, tests in which the bath water is preheated are conducted to obtain a detailed analysis of the heat flux exchanged and the energy accumulated during the phase change processes. In these tests, the encapsulation is first placed in the circular bath to reach the ambient temperature and then placed in the rectangular bath with water preheated to 45 ºC. Only the entirely stainless-steel encapsulation was used for these tests, as the sealant used for attaching the transparent cover in the other encapsulations could not withstand the abrupt temperature change.

The solidification tests represent the opposite process, where energy is released. In these tests, the capsule is preheated in the rectangular thermal bath until it reaches 45 °C and then immersed in the other bath which is at ambient temperature.

In all the tests, water and PCM temperature values are measured by the sensors placed in the bath and in the capsule, respectively. The data is collected using the data acquisition system and processed afterwards.

3. RESULTS

3.1. Assessment of the experimental procedure

In this section, melting tests are conducted with the encapsulation placed vertically, as this is the position in which the most thermal and visual differences are observed, allowing for better conclusions to be drawn.

The first test is conducted with the encapsulations that has the transparent cover and the multipoint probe. The results are shown in Fig. 5. In the graph, three phases are distinguished during the process; the preheating phase, which ranges from ambient temperature until the sensors reach the lower melting point. Then, the phase change occurs, ranging from

the lower to the upper melting temperature, where a less pronounced slope change is observed. Finally, the overheating phase occurs, which ends when the PCM reaches the water temperature.

It is observed that the temperature of the sensors gradually increases over time. The first one that is completely melted is the one located at the top of the encapsulation and the last one is at the bottom. This indicates that the PCM melts downwards, as the liquid phase accumulates in the top due to its lower density. The total time of the process is 50 minutes, when PCM temperature reaches water temperature.

The instants when the sensors are observed through the transparent cover are detected. The photographs of the encapsulation that were taken in these instants are presented in Fig. 6. These time instants are marked on the graph. It is observed that this occurs when the PCM temperature starts to rise rapidly after the phase change, which agrees on the instant when all the PCM around the sensor is melted.

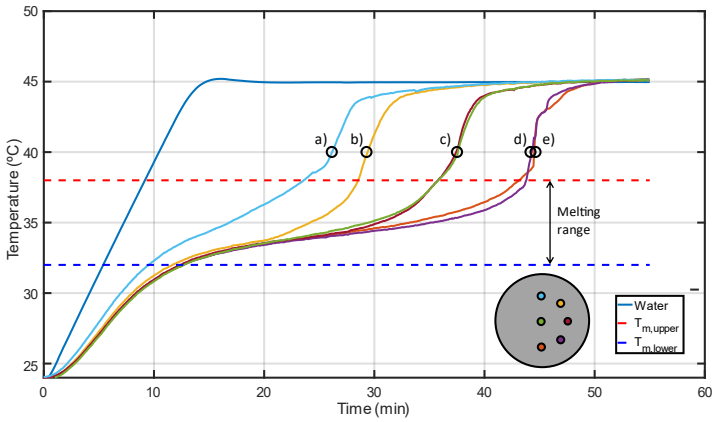

Figure 5. PCM temperature over time in the transparent encapsulation

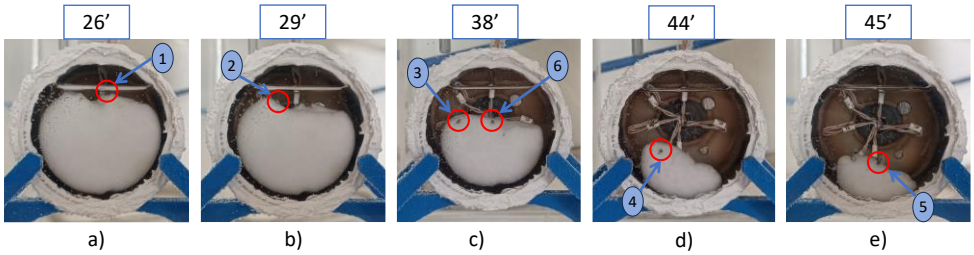

Figure 6. Photographs of the time instants when the sensor are seen through the transparent wall

The melting pattern of the PCM during the test is analyzed through the transparent wall in both encapsulations, with and without probe. The photographs taken at different time instants are shown in Fig. 7. In all of them, the air layer at the top of the encapsulation can be observed, corresponding to 12% of its volume.

The encapsulation on the left is the one with the probe. At minute 15, the PCM is melted along the interior walls of both encapsulations. At minute 20, differences in the patterns start to become noticeable. In the encapsulation without the probe, the solid PCM is at the bottom and the liquid PCM is at the top, due to the difference in densities between the two phases. In the encapsulation with the probe, the PCM remains centred, and approximately the same amount of solid PCM as in the previous photograph is observed. This is because the probe holds the solid PCM, altering the melting pattern from the natural convection-dominated pattern. Consequently, this delays the melting of the solid PCM by approximately 15 minutes, as it remains mostly in the central area and cannot sink to the bottom of the encapsulation until it is completely detached from the sensors. A similar effect is observed in the study conducted by Tan in 2008, where thermocouples were placed inside a single tube within a spherical glass encapsulation. This phenomenon is known as constrained melting. With six sensors, this effect becomes more evident.

It is significant to note that the moment when all the sensors have reached the upper melting temperature, approximately at minute 45 according to Fig. 5, does not correspond to the instant when the PCM is completely melted, which occurs 5 minutes later. This coincides with the instant when all the sensors reach the water temperature. Hence, in subsequent tests, this delay will be taken into account when calculating the total time of the test.

Subsequently, a test is conducted to study the effect of the methacrylate used as transparent cover in the encapsulations due to its low thermal conductivity of 0.2 W/(K*m). This test consists of comparing the temperature values obtained in the encapsulation with this cover to those obtained in the encapsulation made entirely of stainless steel, when both are placed in the thermal bath.

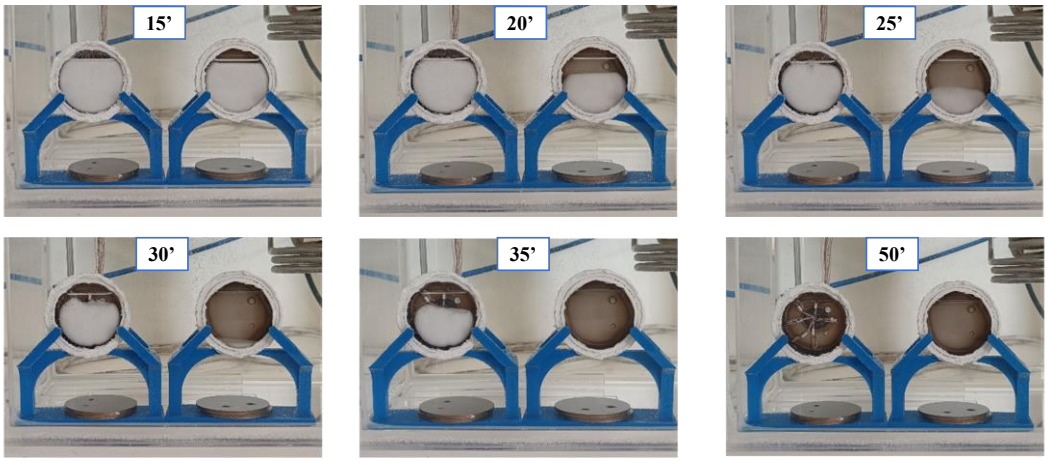

Figure 7. Photographs of the PCM melting pattern evolution in encapsulations with (left) and without probe (right)

The results of this test are graphically represented in Fig. 8, where the temperatures of the probes in the steel encapsulation (solid line) and the transparent encapsulation (dotted line) are shown, along with the water temperature. It is observed that the graphs for both encapsulations follow the same trend, but the steel encapsulation heats earlier due to its higher conductivity. Therefore, it is concluded that the insertion of a transparent cover affects the melting of the PCM inside the encapsulation, slowing down the melting process by approximately 5 minutes.

The tests in this section have demonstrated that the use of probes to measure temperatures inside the encapsulation significantly affects the melting time, as does the incorporation of a methacrylate cover. Therefore, it can be concluded that the measurement methods employed in this study to experimentally determine the behavior of the encapsulated PCM will affect it to some extent. Nonetheless, this has provided an approximation of how the PCM behaves within the encapsulation, both quantitatively with the thermal results and qualitatively with the visual results. Therefore, it can be assumed that the total melting time in the described stainless-steel encapsulation without a probe and without a transparent cover is about 30 minutes.

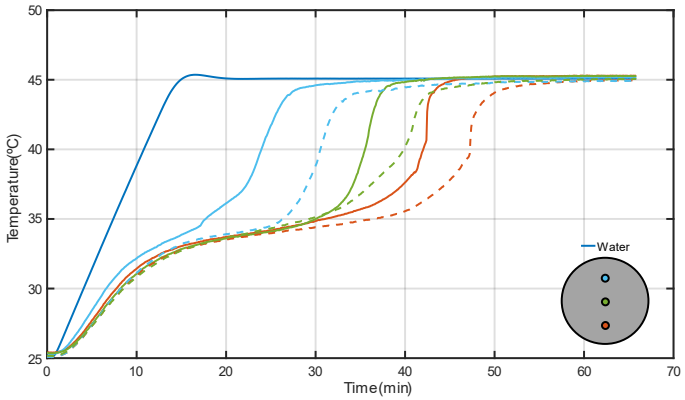

Figure 8. Comparison of the PCM temperature in the stainless-steel encapsulation (solid line) and in the transparent encapsulation (dotted line).

3.2. Analysis of the phase change processes

Based on the conclusions drawn from the previous tests, in this section the analysis of the energy stored and released during the phase change processes of the encapsulated PCM is done. Melting and solidification tests are conducted, with the stainless-steel encapsulation placed both vertically and horizontally.

3.2.1. Melting tests

The temperature results of the test when the encapsulation is in vertical are shown in Fig. 9a. It can be observed that the sensors detect the gradual increase in PCM temperature from the top to the bottom of the encapsulation, similar to what was observed in Fig. 5. The three phases are distinguished in this test too. Comparing the graphs of both tests, it is noted that they follow the same trend. The difference lies in the total time of the test, which is around 40 minutes in these

tests, whereas it is 50 minutes in the previous ones, where the water was not preheated. The liquid fraction of this test is presented in Fig. 9b. It is observed how it progressively increases from 0 to 1 during the phase change. With this graph, the phase change time can be determined, which is 30 minutes.

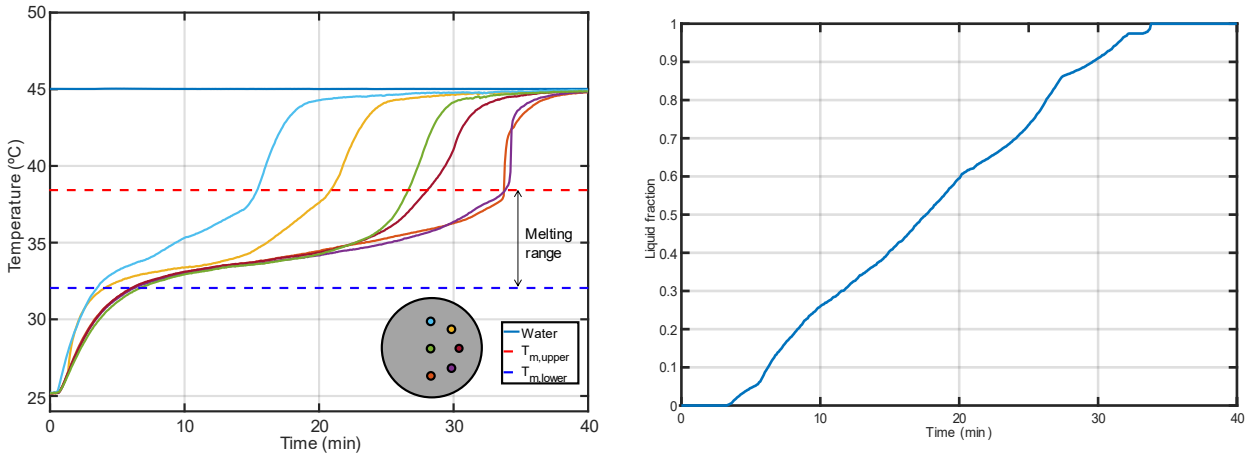

a) b)

Figure 9. a) PCM temperature over time in the stainless-steel encapsulation placed in vertical during the melting tests b) Liquid fraction

Figure 10a shows the results of the tests when placing the encapsulation in horizontal. The three heating phases are distinguished in this test too. It is observed that the temperature of the sensors located on the semicircumference follows a similar trend and heats up earlier than the central sensor. This is because they are closer to the side wall of the encapsulation. Based on these results, it is also noted the differences in the temperature evolution between horizontal and vertical position. In the horizontal encapsulation, the temperature increase is almost uniform, while in the vertical encapsulation, the sensors heat up progressively, with a temporal difference between them. Nevertheless, the total time of both of tests is the same, 40 minutes. The liquid fraction of this test is presented in Fig. 10b. With this graph, the phase change time can be determined, which is 25 minutes.

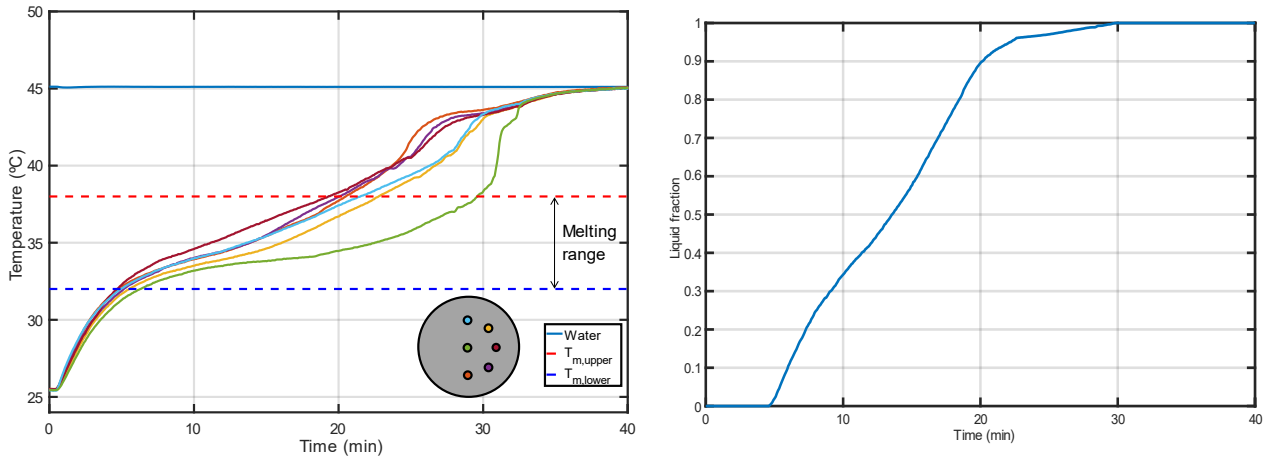

a) b)

Figure 10. a) PCM temperature over time in the stainless-steel encapsulation placed in horizontal during the melting tests b) Liquid fraction

Subsequently, the analysis of the energy stored by the PCM is done. The calculation of the global energy (Eq. (3)) in the melting test is 9695.5 J, which is now compared with the energy calculated by integrating the heat flux.

The PCM heat flux calculated at several time instants during the process is represented in both vertical and horizontal positions in Fig. 11, along with the moving average, so an estimation of these data is calculated. In both cases, it is observed that the heat flux starts from 0 and then abruptly increases when the phase change begins, remaining constant within a range of values. Then, when the phase change ends, the heat flux decreases again until it becomes 0. This indicates that the majority of the energy is stored during the phase change.

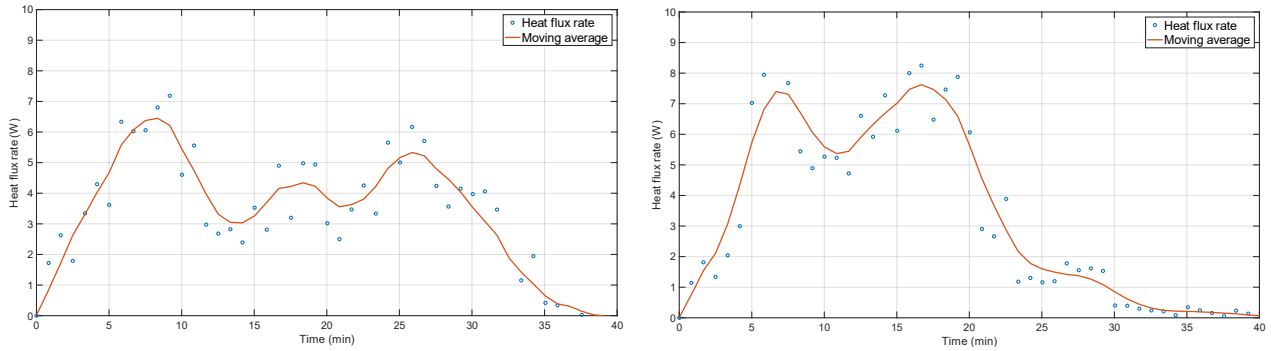

Figure 11. Heat flux of the melting tests a) Vertical position b) Horizontal position

The energy stored at each time instant is shown in Fig. 12, from which the accumulated energy in the test and the energy rate in each phase are obtained. These rates are calculated assuming that the energy follows a linear trend in each phase, thus the rate is determined from the initial and final values of time and energy of each phase. The values are included in Table 2. If the energy accumulated in the PCM is added to the energy accumulated in the steel, which is 1120.6 J, the total energy obtained is 9470.6 J in the vertical position and 9745.6 J in the horizontal position. This corresponds to an error relative to the global energy of 2.3% and 0.5%, respectively. Therefore, it is considered that the calculation of energy by integration is valid, as the results are of the same order of magnitude as the global equation.

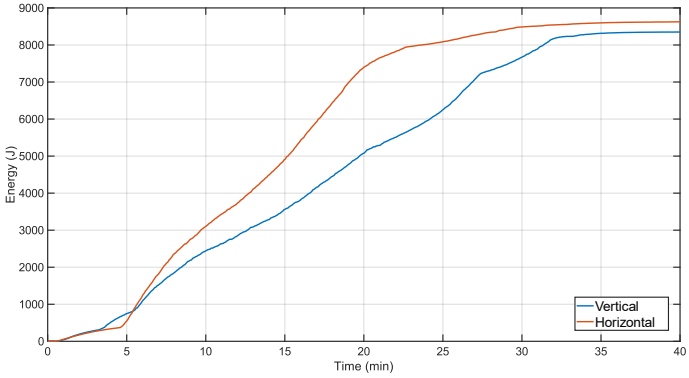

Figure 12. Accumulated stored energy during the melting tests

Table 2. Accumulated energy and energy rates of the melting tests

Energy calculation [units]	Vertical position	Horizontal position
Accumulated energy [J]	8350	8625
Energy rate during preheating [J/min]	96.1	83.83
Energy rate during phase change [J/min]	263.7	322.2
Energy rate during overheating [J/min]	1.3	8.1

3.2.2. Solidification tests

The results of the solidification test in the vertical position are shown in Fig. 13a. Similar to the melting tests, three phases are observed: in the stage before the phase change, the precooling, the temperature drops rapidly until it reaches the upper solidification temperature. Here, the phase change begins, marked by a significant change in the slope, until it reaches the lower solidification temperature. In the third stage, the subcooling, the PCM continues to cool until it reaches the water temperature.

It is observed that the first sensor that starts to solidify is the one located at the top, as it is closest to the air layer. Subsequently, the sensors located on the periphery solidify in an approximately uniform way, as it is supposed that firstly PCM solidifies over the inner walls of the encapsulation. Then, the last one to solidify is the sensor in the center.

The total time of the process is about 80 minutes, twice as long as the melting test. This is because conduction phenomena dominate in the solidification process, unlike the melting process, where convection phenomena dominate. Since paraffin has low thermal conductivity (0.2 W/(m*K), according to the manufacturer), the solidification process is slower. The liquid fraction of this test is presented in Fig. 13b. Unlike in Figure 9b, the liquid fraction goes from 1 to 0, as it starts in the liquid phase and then decreases progressively during the phase change. With this graph, the phase change time can be determined, which is 55 minutes.

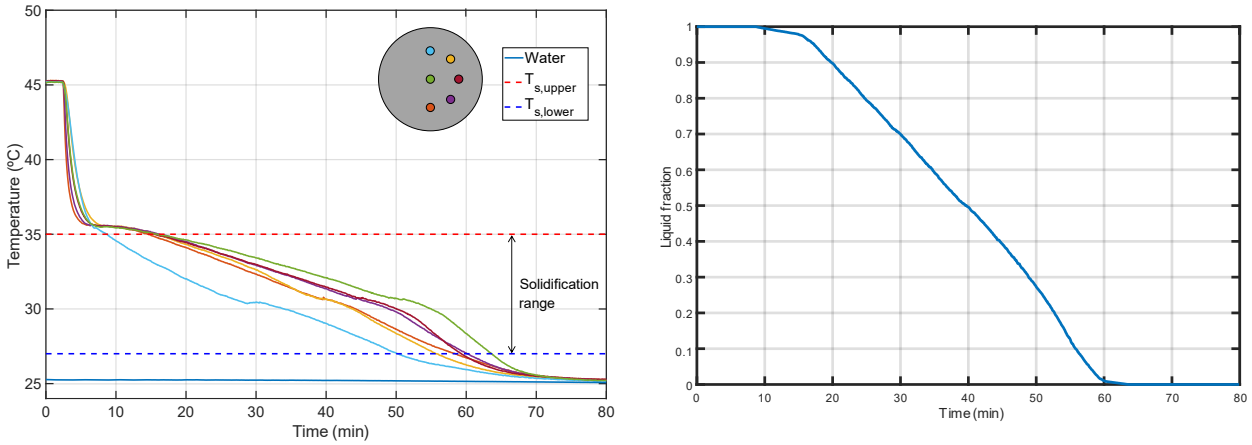

a) b)

Figure 13. a) PCM temperature over time in the stainless-steel encapsulation placed in vertical during the solidification test b) Liquid fraction

The results of the test with the encapsulation placed horizontally are shown in Fig. 14a. In this case, similar to the melting process in the horizontal position, the sensors located on the outer part solidify uniformly first, and the central sensor solidifies last. As in the vertical position, the test also takes longer than the melting tests, approximately 70 minutes. The liquid fraction of this test is presented in Fig. 14b. With this graph, the phase change time can be determined, which is 50 minutes.

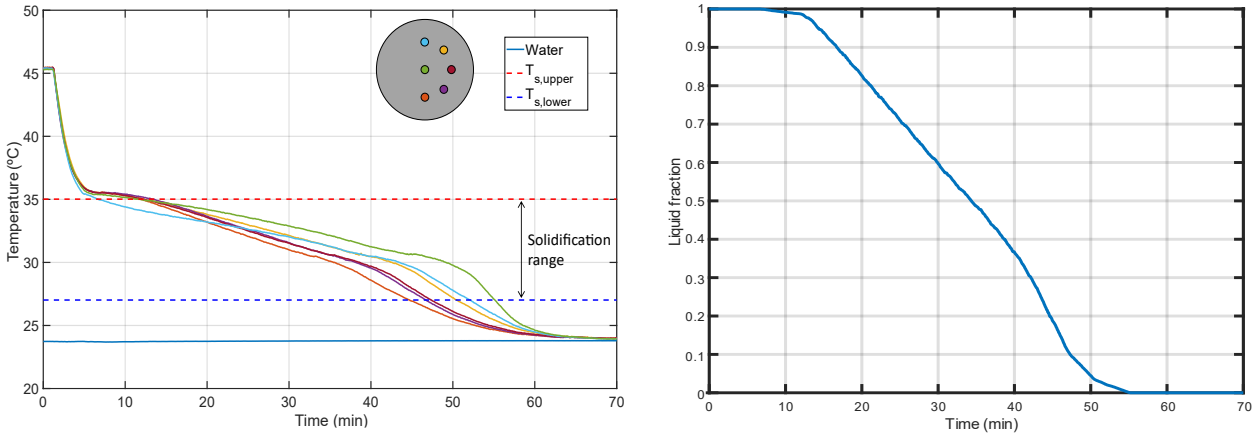

a) b)

Figure 14. a) PCM temperature over time in the stainless-steel encapsulation placed in horizontal during the solidification test b) Liquid fraction

Analogous to the melting tests, the released energy is analyzed below. The global energy calculated with Eq. (3) is 9815.4 J. The heat flux values at several time instants during the process in both positions are represented along with the moving average in Fig. 15. In this case, during the pre-cooling phase, a peak is observed due to the abrupt decrease of temperature during this phase. Then, it increases again and even more during the phase change, remaining constant within a range of values, until it becomes nearly zero during the subcooling phase. Again, the majority of the energy is released during the phase change. The stored energy at each time instant is shown in Fig. 16. In Table 3, the values of released energy and the rate of energy released in each phase of the process are presented.

Adding to the PCM released energy in each position the stainless-steel energy, it is obtained 9730.6 J for the vertical position and 9345.6 J for the horizontal position. This corresponds to an error relative to the calculated global energy of 0.8% and 4.7%, respectively. Therefore, it is considered that the calculation of energy by integration is valid, as the results are of the same order of magnitude as the global equation.

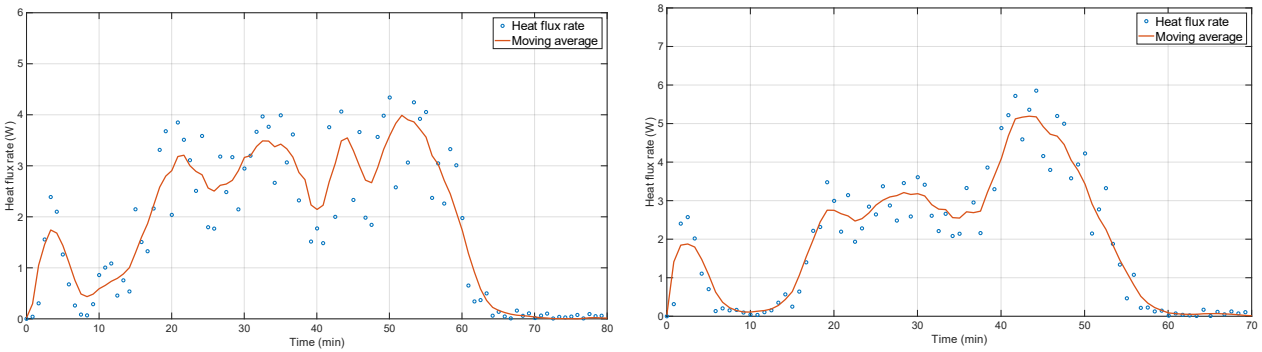

Figure 15. Heat flux of the solidification tests a) Vertical position b) Horizontal position

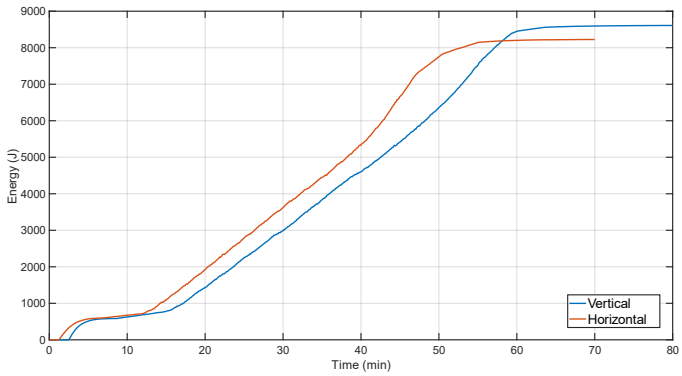

Figure 16. Accumulated released energy during the solidification tests

Table 3. Accumulated energy and energy rates of the solidification tests

Energy calculation [units]	Vertical position	Horizontal position
Accumulated energy [J]	8610	8225
Energy rate during precooling [J/min]	66.3	49.8
Energy rate during phase change [J/min]	145.4	171.7
Energy rate during subcooling [J/min]	1.74	3.3

4. CONCLUSIONS

In this study, the phase change processes of PCM encapsulated in a stainless-steel cylinder have been analyzed, using RT35HC paraffin from Rubitherm as the PCM. Firstly, the properties of the PCM have been measured to obtain more accurate values than those provided by the manufacturer, using DSC analysis and other measurement techniques. Afterwards, the measurement methods used to understand the behavior of the encapsulated PCM have been assessed. It has been concluded that both the multi-point probe inside the encapsulation to measure the temperature field and the transparent cover to visualize its interior affect the phase change processes of the encapsulated PCM. The melting pattern is altered and the melting time is prolonged. However, these techniques have provided a better understanding of the behavior of the PCM in a cylindrical encapsulation and an approximate value for the melting time during the charging process.

Subsequently, the melting and solidification processes of the PCM have been analyzed with the encapsulation placed in both vertical and horizontal positions. It has been found that the melting time is independent of the encapsulation position, and the same practically happens in the solidification process. Nevertheless, the solidification time is nearly

double that of melting since the conduction dominates during solidification process and paraffins has very low thermal conductivity, while convection dominates during melting.

The heat flux exchanged in each test has been obtained and the accumulated energy has been calculated, first using a global method and second by integrating the heat flux. Despite the rough assumptions that have been made, it has been concluded that the integration method is valid as the results agree on the global calculation, so an order of magnitude of the energy stored or released by the encapsulation and the energy rate during the phases of the process has been obtained.

5. ACKNOWLEDGEMENTS

This work was funded by the European Regional Development Fund, Ministerio de Ciencia e Innovación – Agencia Estatal de Investigación and European Union NextGenerationEU/PRTR for the project "Enhanced Solar-System for Thermal Hybrid Energy Storage" (PID2022-141649OB-C21).

6. REFERENCES

Archibold, A.R., Gonzalez-Aguilar, J., Rahman, M.M., Goswami, D.Y., Romero, M. and Stefanakos E.K., 2014. "The melting process of storage materials with relatively high phase change temperatures in partially filled spherical shells", *Applied Energy*, vol. 116, pp. 243-252.

Assis, E., Katsman, L., Ziskind, G. and Letan, R., 2007. "Numerical and experimental study of melting in a spherical shell", *International Journal of Heat and Mass Transfer*, vol. 50, pp. 1790-1804.

Boroojerdian, A., Nemati, H. and Selahi, E, 2023. "Direct and non-contact measurement of liquid fraction in unconstrained encapsulated PCM melting", *Energy*, vol. 284, 129359.

Cheng, Z. and Zhai, X., 2017. "Thermal performance analysis of a novel PCM capsule in red blood cell shape", *Applied Thermal Engineering*, vol 120, pp. 130-137.

El Aziz, Y. A., 2022. "Renewables 2022 Global Status Report Germany Factsheet", *Report,*

Hernández Ballester, Marta, 2023. *Diseño, construcción y caracterización experimental de un prototipo de almacenamiento de energía térmica híbrido con material de cambio de fase encapsulado*, Final Master Thesis, Polytechnic University of Cartagena, Spain.

Issa, O. O. and Thirunavukkarasu, V., 2024. "Experimental study on charging and discharging behavior of PCM encapsulations for thermal energy storage of concentrating solar power system", *Journal of Energy Storage*, vol. 85, 111071.

Kahwaji, S., Johnson, M. B., Kheirabadi, A.C., Groulx, D. and White, M. A., 2018. "A comprehensive study of properties of paraffin phase change materials for solar thermal energy storage and thermal management applications", *Energy*, vol. 162, pp. 1169-1182.

Kumar, A. and Saha, S.K., 2022. "Thermal and structural characterizations of packed bed thermal energy storage with cylindrical micro-encapsulated phase change materials", *Journal of Energy Storage*, vol. 48, 103948.

Li, W., Wang, Y.- H., and Kong, C.- C., 2015. "Experimental study on melting/solidification and thermal conductivity enhancement of phase change material inside a sphere", *International Communications in Heat and Mass Transfer*, vol. 68, pp. 276-282.

Liu, L., Zhang, X. and Lin, X., 2022. "Experimental investigations on the thermal performance and phase change hysteresis of low-temperature paraffin/MWCNTs/SDBS nanocomposite via dynamic DSC method", *Renewable Energy*, vol. 187, pp. 572-585.

Majumdar, R. and Saha, K., 2020. "Computational study of performance of cascaded multi-layered packed-bed thermal energy storage for high temperature applications", *Journal of Energy Storage*, vol. 32, 101930.

Mekaddem, N., Ben-Ali, S., Fois, M., and Hannachi, A., 2024. "Development and characterization of advanced paraffin plaster composite for building energy storage", *Journal of Building Engineering*, vol 84, 108603.

Tan, F.L., 2008. "Constrained and unconstrained melting inside a sphere". *International Communications in Heat and Mass Transfer*, vol 35, pp. 466-475.

Teather, k. and Siddiqui, K., 2023. "Non-invasive measurement of the temperature field of a phase change material (PCM) using thermal imaging", *Experimental Thermal and Fluid Science*, vol. 148, 110991

Veerappan, M., Kalaiselvam, S., Iniyan, S, and Goic, R., 2009. "Phase change characteristic study of spherical PCMs in solar energy storage", *Solar Energy*, vol. 83, pp. 1245-1252.

Xu, T., Humire, E. N., Trevisan, S., Ignatowicz, M., Sawalha, S. and Chiu, J. NW., 2022. "Experimental and numerical investigation of a latent heat thermal energy storage unit with ellipsoidal macro-encapsulation", *Energy*, vol. 238, 121828.

Yang, L., Zhang, X. and Xu, G., 2014. "Thermal performance of a solar storage packed bed using spherical capsules filled with PCM having different melting points", *Energy and Buildings*, vol. 68, pp. 639-646.